Ceramics International 44 (2018) 10781–10789

Contents lists available at ScienceDirect

Ceramics International

journal homepage: www.elsevier.com/locate/ceramint

Photoluminescence behavior on Sr^{2+} modified $CaCu_3Ti_4O_{12}$ based ceramics

S. Orrego[a], J.A. Cortés[a,*], R.A.C. Amoresi[b], A.Z. Simões[a], M.A. Ramírez[a]

[a] São Paulo State University – UNESP, Faculty of Engineering of Guaratinguetá, Av. Dr Ariberto Pereira da Cunha 333, Portal das Colinas, 12.516-410 Guaratinguetá, SP, Brazil

[b] São Paulo State University – UNESP – Chemistry Institute, Rua Prof. Francisco Degni, 55, Quitandinha, 14800-060 Araraquara, SP, Brazil

ARTICLE INFO

Keywords:
$CaCu_3Ti_4O_{12}$
Solid-state reaction
Photoluminescent behavior

ABSTRACT

Sr^{2+} modified $CaSr_xCu_{3-x}Ti_4O_{12}$ ceramic powders with x = ranging from 0.00 to 3.00 were prepared by solid-state reaction. The effects of Sr^{2+} CCTO powders were evaluated by X-ray diffraction (XRD) with Rietveld refinement revealing a mixture of multiple phases. The Raman spectroscopy analysis pointed out that Sr^{2+} addition produces an emission in the blue region, associated to TiO_6 clusters. Optical properties by means of PL analysis showed emission near to blue region for the samples with x = 0.00, x = 0.15, x = 0.30, corresponding to oxygen vacancies. The emission in the violet region is associated to deep defects while emission in the other samples is linked to shallow defects typical of disordered crystalline structures. Less prominent emission in the green region with the increase of Sr^{2+} corresponds to less self-trapped charges, less interaction between electron and hole, and donor–acceptor recombination.

1. Introduction

Ceramics based on $CaCu_3Ti_4O_{12}$ (CCTO) have awakened the scientific attention due to their giant dielectric constant (ε), discovered by Subramanian et al. [1] in 2000. In 2004, Chung et al. [2] reported the non-ohmic property of CCTO. In order to understand the multifunctional behavior of such system, different researches are being conducted [3–13]. Several models have been proposed to explain the dielectric response such as: IBLC model (Internal Barrier Layer Capacitor) [14–16], and the NBLC model (Nanosized Barrier Layer Capacitor) [12,17]. On the other hand, compared with systems that also present dielectric behavior, the CCTO has a giant dielectric constant, which is generated by an extrinsic nature, related to the processing and to small stoichiometry changes [18–20]. The CCTO system is represented by $AA'_3B_4O_{12}$, where A' is the lattice modifier and the B is the lattice former.

Photoluminescence (PL) emission is a powerful tool employed to elucidate the properties of different materials with perovskite structure, being closely related to the crystal structure and its corresponding distorted metal–oxygen polyhedrons. In particular, many titanates present structures with lower symmetries which under ambient conditions could derive the rotation or tilting of regular, rigid octahedrons resulting in the presence of distorted TiO_6 clusters [21–23]. Although the structure is distorted, the rotation/tilting of the octahedral framework does not disrupt the corner-sharing connectivity.

The PL response is being studied by different researchers, due to the applicability in optics devices. This has already been reported in different materials with a perovskite structure [21–26], among them the CTO [27] CCTO [22,28–31] and CCTO/CTO [32]. Usually, the PL behavior is attributed to multiphonon processes, i.e., a system in which relaxation occurs through several paths located in states of energy above the valence band and below the conduction band [33]. The degree of symmetry and crystallinity has influence on PL emission. Materials with high degree of symmetry present PL emission through electronic states created within the band gap of the disordered cluster in the structure [23]. The PL property of the CCTO is mainly associated with the presence of oxygen vacancies in the $[TiO_6]$ clusters generating clusters of type $[TiO_5.V_o^2]$ [29,30,34–36]. This type of vacancies generates energy inside the gaps of the material, altering the movement of electrons between different levels [29]. As reported by Moura et al., the band gap of CCTO decreased and consequently an increase in the PL emission is noted with the increase of Zr^{4+} doping, producing short-range distortion in the perovskite structure due to the formation of $[TiO_5/TiO_6]$ cluster [37]. Some studies analyzed the substitution of Ca^{2+} by Sr^{2+} in the CCTO [35,38], but few studies have emphasized the role of partial and total substitutions of the Cu^{2+} ions. The changes in the PL property of the CCTO phase with the partial and total substitution of Cu^{2+} by Sr^{+2} in the presence of SCTO phase have been reported by a small number of authors [39–41]. Therefore, our work is focused to explain the photoluminescent response of crystalline ceramics with multiple phases obtained through solid-state reaction. Our goal is devoted to some critical steps: (a) Phase formation by a study

* Corresponding author.
E-mail address: joalcosu.nal@gmail.com (J.A. Cortés).

https://doi.org/10.1016/j.ceramint.2018.03.116
Received 19 December 2017; Received in revised form 13 March 2018; Accepted 13 March 2018
Available online 14 March 2018
0272-8842/ Published by Elsevier Ltd.

based on thermal analyses and Rietveld refinement, (b) Correlation between the wavelength emission with the Sr^{2+} content evidenced by the photon modes of the multiple phases and (c) The possible origin of PL behavior caused by Ti^{4+} off-center, which is common to TiO_6 clusters.

2. Experimental procedure

2.1. Synthesis

Ceramic powders based on $CaSr_xCu_{3-x}Ti_4O_{12}$ ($0.00 \leq x \leq 3.0$), specifically with x values of 0.00, 0.15, 0.30, 1.50, 2.70 and 3.00, were prepared using solid-state reaction. The reagents used were $CaCO_3$ (Aldrich), CuO (Aldrich), TiO_2 (Aldrich) and $SrCO_3$ (Aldrich), all of them of analytic grade (99.99% of purity). To obtain homogeneity of the powder, the reagents were mechanically mixture in a rotary mill for 24 h using a polyethylene pot, zirconium balls stabilized with yttrium and isopropyl alcohol. After drying in stove for 12 h, the powder was deagglomerated in mortar, granulated in sieve of 200 mesh and calcinated at 1050 °C for 12 h. The thermogravimetric studies were made using a TG-DTA of vertical cell, Netzsch, STA 409 model.

2.2. Characterizations

Phase analysis of the powders was carried out using the X-ray diffractometry technique by a rotatory diffractometer (RIGAKU®, model RINT2000) operated at 50 kV/120 mA and using copper Kα radiation. The study was performed in the range of 10–120, with steps of 0.02 grades. The crystalline structure and Rietveld refinement were acquired with the software's Mercury 3.8 and Diamond 4.40 and GSAS free version. The phases were identified and refined based on the Inorganic Crystal Structure Database (ICSD). The Raman spectroscopy characterization was obtained by LabRAM iHR550 Horiba Jobin Yvon spectrometer with a laser 514 nm wavelength, as an excitation source, and spectral resolution of 1 cm^{-1}, with 40 scans, in the range 100–800 cm^{-1}, coupled to a CCD detector.

The UV–vis spectrum was obtained using a photo spectrometer Cary 5 G (Varian, USA) in a diffusive reflection mode. To calculate the gap energy value (E_{gap}) the Kubelka-Munk method was used [42]. This strategy is based on the counts with the scattering phenomena of the radiation with the matter, allowing a more precise value of gap energy. This value is related with the absorbance of the material and the photons energy by the Eq. (1):

$$ah\nu = C_1(R_\infty(h\nu - E_{gap})^n) \quad (1)$$

where, α is the linear coefficient of absorbance, hν is the photons energy, C_1 is a constant, R_∞ is the reflectance when the sample is taken as infinitely thick, E_{gap} is the optical energy gap and n is a constant associated to the different types of electronic transitions ($n = ½$ to direct transitions and $n = 2$ to indirect transitions). The photoluminescent spectrum was built using a thermal monochromator monospec Jarrel-Ash and a photomultiplier Hamamatsu R446. A laser (Coherent Innova) of wavelength 350.7 nm (2.57 eV), with 200 mW of power was used. All measurements were performed at room temperature.

3. Results and discussion

3.1. Thermal analysis

Fig. 1(a) shows the thermogravimetric analysis (TG) to all powders synthesized through solid-state reaction. $CaSr_xCu_{3-x}Ti_4O_{12}$ sample with x = 0.00 shows a single mass loss in the temperature range from 600 °C at 850 °C due to the $CaCO_3$ decomposition. Samples with low Sr^{2+} contents (x = 0.15–0.30) show two mass loss stages. The first one begins at 230 °C and can be attributed to the output of water adsorbed by the carbonates while the second stage at range 650–850 °C is caused by

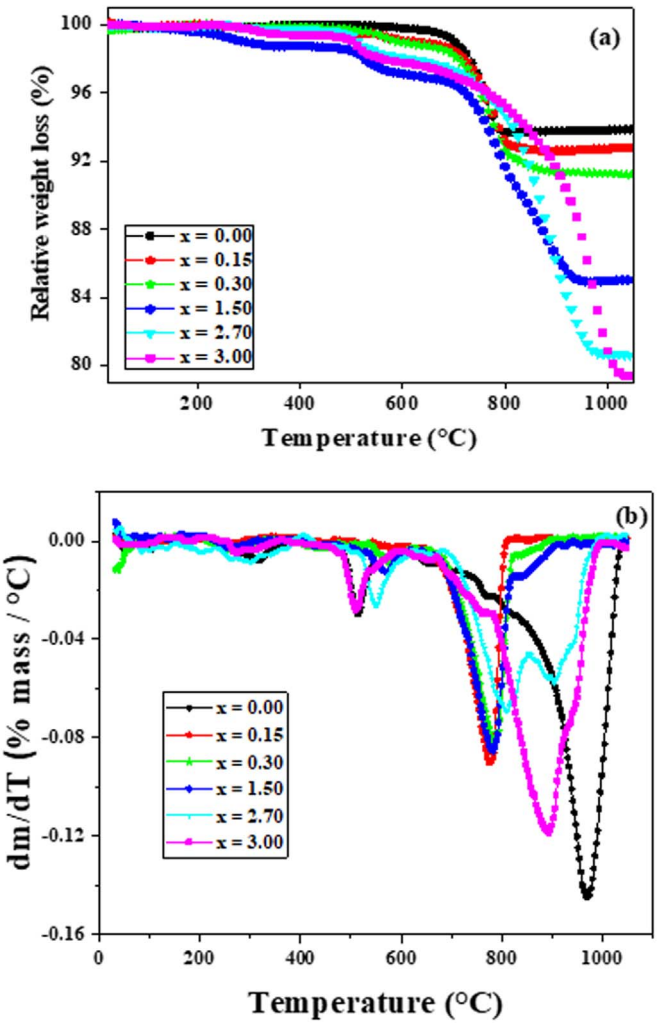

Fig. 1. (a) Thermogravimetric graphics and (b) derivative of the thermogravimetric analysis of ceramic powders based on $CaSr_xCu_{3-x}Ti_4O_{12}$ ($0.00 \leq x \leq 3.00$).

the release of CO_2 from $CaCO_3$ as it is known that $SrCO_3$ decomposes between the 875 °C and 1035 °C [43,44]. On the other hand, the samples with x = 1.50–3.00 illustrate four mass loss stages. Two stages are identical as mentioned above while the other two can be explained as follows: At 450 °C the release of CO occurs, and near 880 °C, CO_2 goes out of $SrCO_3$ [43]. Such samples revealed a 20% of mass loss at 1030 °C, indicating that high calcination temperatures are required to obtain such crystalline phases. The Fig. 1(b) shows the DTG curves where two distinct events can be noted. The first one occurs between 480 and 580 °C, being associated to the release of CO_2 coming from both carbonates [45,46]. The second one takes place from 700 until 1050 °C and can be explained by the complete decomposition of $CaCO_3$ and $SrCO_3$. For the samples with x = 2.70 and x = 3.00 the second event is shifted to higher temperatures, being related to phase changes corresponding to strontium carbonate [43]. Thus, for comparative terms, 1050 °C was chosen as the calcination temperature, ensuring no mass loss.

3.2. X-ray diffractometry

Fig. 2 shows the X-ray diffraction patterns. It can be observed that the sample with x = 0.00 (Fig. 2a) presented only the CCTO phase (ICSD card 91–097), corresponding to a cubic perovskite structure with space group *Im-3*, while the sample with x = 3.00 (Fig. 2f) presented only SCTO phase (ICSD card 29–0861) with orthorhombic structure (Table 1). This phase belongs in the space group *Ibmm*, as already

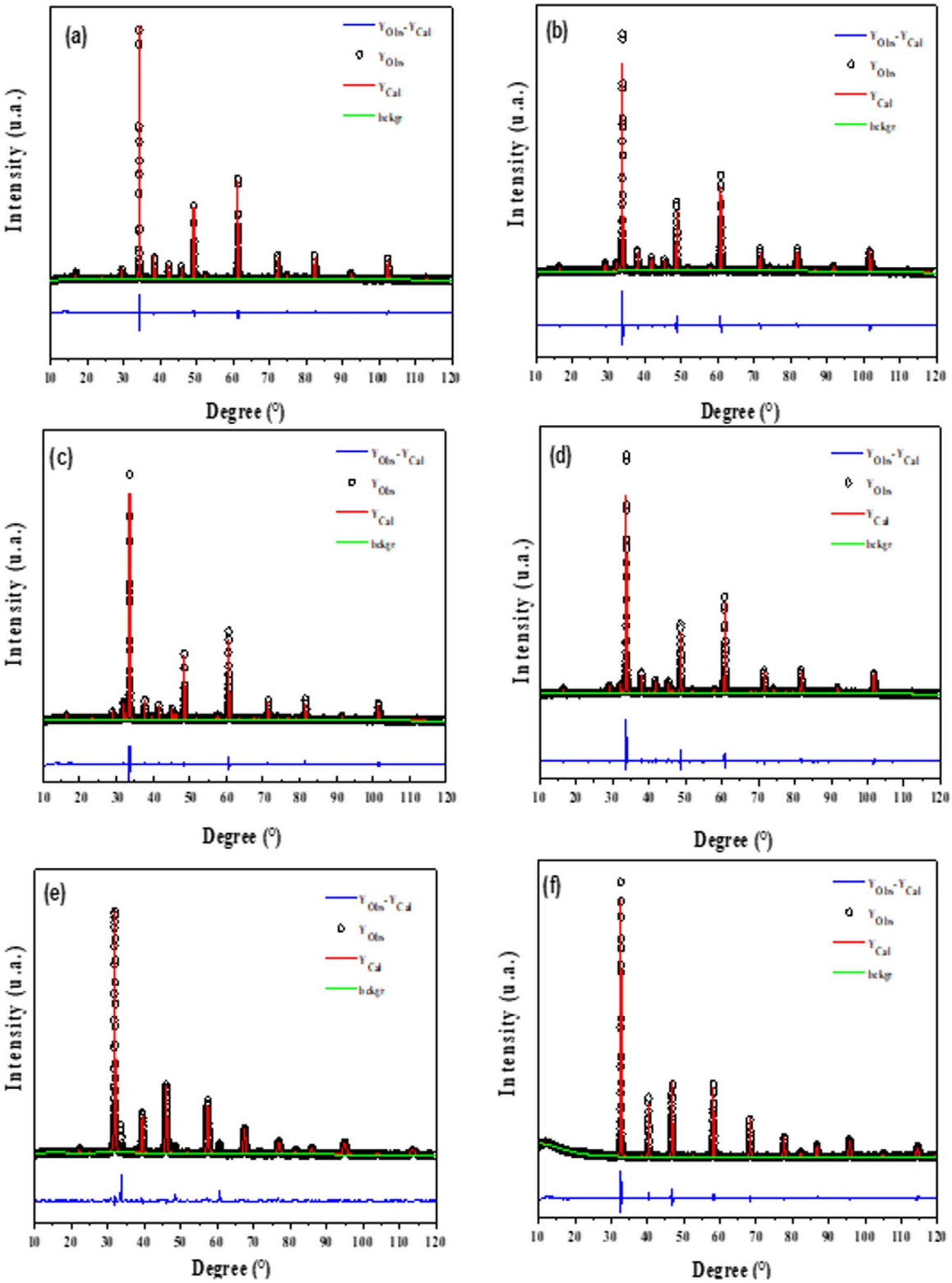

Fig. 2. X-ray diffraction of ceramic powders based on $CaSr_xCu_{3-x}Ti_4O_{12}$ where (a) x = 0.00; (b) x = 0.15; (c) x = 0.30; (d) x = 1.50; (e) x = 2.70 and (f) x = 3.00.

shown in the literature [46]. The presence of CCTO, SCTO and CTO (ICSD card 62–149) with space group *Pbnm* was evidenced in the samples with x = 0.15, 0.30, 1.50 and 2.70 (Fig. 2b–e). In this study, the Rietveld refinement technique was used to investigate the crystal structure of the all examined samples. The data were collected from powders calcinated at 1050 °C for 12 h obtained through solid-state reaction in the conventional furnace. The crystal structure was used as a tool for structural refinement; the results showed that the oxygen octahedron was heavily tilted and the Cu^{2+} cations adopted a four-fold square-planar coordination. The structure refinement data for all samples were presented and the χ^2 values lead to conclude that the refinement was credible in accordance with released literature. Table I illustrates the R_{wp}, R_{exp}, unit cell volume (V), χ^2 and the percentage of each phase. We noted that the sample with x = 0.15 shows the CCTO

Table 1
Structural parameters of samples of $CaSr_xCu_{3-x}Ti_4O_{12}$, with x = 0.00, 0.15, 0.30, 1.50, 2.70 and 3.00.

Samples	$CaCu_3Ti_4O_{12}$ percentage (%)		$Sr_{.75}Ca_{.25}TiO_3$ percentage (%)				$CaTiO_3$ percentage (%)				Rietveld values		
	a (Å)	Volume (Å^3)	a (Å)	b (Å)	c (Å)	Volume (Å^3)	a (Å)	b (Å)	c (Å)	Volume (Å^3)	R_p	R_{wp}	χ^2
x = 0.00	100		0				0				2.82	3.85	2.766
	7.394	404.26	0	0	0	0	0	0	0	0			
x = 0.15	96.60		3.40				0				3.72	5.51	4.964
	7.422	408.83	5.342	5.480	7.773	233.97	0	0	0	0			
x = 0.30	72.48		7.90				19.62				3.19	4.46	3.659
	7.422	408.79	5.485	5.50	7.791	235.06	5.246	5.270	7.418	205.11			
x = 1.50	40.57		33.96				25.46				4.29	6.12	5.411
	7.397	404.77	5.485	5.501	7.798	235.31	5.502	5.559	7.741	236.78			
x = 2.70	5.75		65.04				29.21				5.30	7.07	5.557
	7.397	404.67	5.497	5.506	7.805	236.67	5.452	5.482	7.781	232.59			
x = 3.0	0		100				0				5.74	7.65	5.771
	0	0	5.492	5.501	7.798	235.60	0	0	0	0			

(96.60%) and SCTO (3.40%) phases indicating that Sr^{2+} exceeds the limits of solid substitution. The sample with x = 0.30 showed three phases in equilibrium, denoted as CCTO (72.48%), SCTO (7.90%) and CTO (19.62%). As already shown in literature [47], the CTO phase is originated from the copper deficiency in CCTO. Different proportions of the same phases presenting CCTO (40.57%), SCTO (33.96%) and CTO (25.46%) were obtained for the sample with x = 1.50. In the case of the sample with x = 2.70 is evident the presence of CCTO, CTO and SCTO phases, with the largest percentage being the SCTO phase (65.04%). Finally, the sample with x = 3.00 presents SCTO phase as a single phase, indicating that Sr^{2+} completely replaces calcium on the CTO phase.

3.3. Raman spectroscopy

Fig. 3a shows the Raman spectrum of all samples, where 13 different Raman modes (P1-P13), all associated to TiO_6 clusters can be noted. P7, P8 and P9 Raman modes could be identified for the compositions with x = 0.00, 0.15 and 0.30, corresponding to wavenumbers near to 445 cm^{-1} (P7 mode), 506 cm^{-1} (P8 mode), and 572 cm^{-1} (P9 mode). All these modes could be addressed to TiO_6 clusters in the T_g and A_g symmetries. Besides that, P7 and P8 Raman modes shift to an

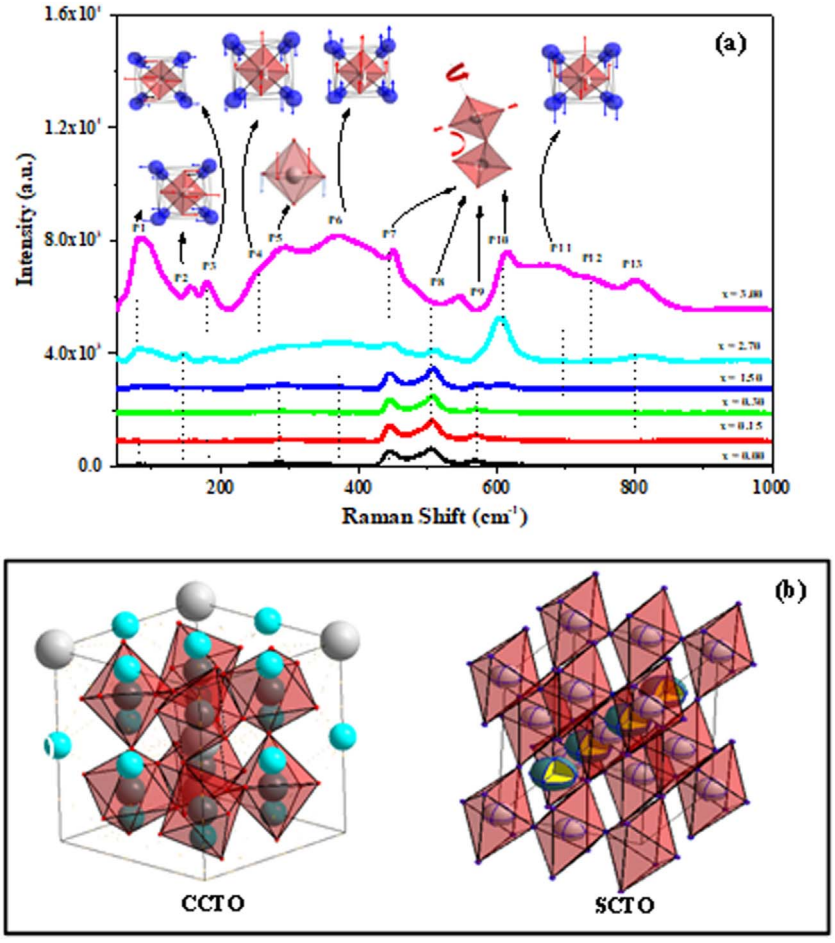

Fig. 3. a) Raman spectrum of ceramic powders based on $CaSr_xCu_{3-x}Ti_4O_{12}$ ($0.00 \leq x \leq 3.00$). b) Representation of the crystalline structures of CCTO and SCTO.

Table 2
Experimental vibrational modes of samples of $CaSr_xCu_{3-x}Ti_4O_{12}$, compared with literature values.

s	Mode$CaSr_xCu_{3-x}Ti_4O_{12}$						Literature
	x = 000	x = 0.15	x = 0.30	x = 1.50	x = 2.0	x = 3.00	[48,58]
Ag_1 (cm^{-1})	442	443	443	447	447	447	445
Ag_2 (cm^{-1})	510	509	509	509	510	509	512
Fg_1 (cm^{-1})	573	573	573	574	574	574	572

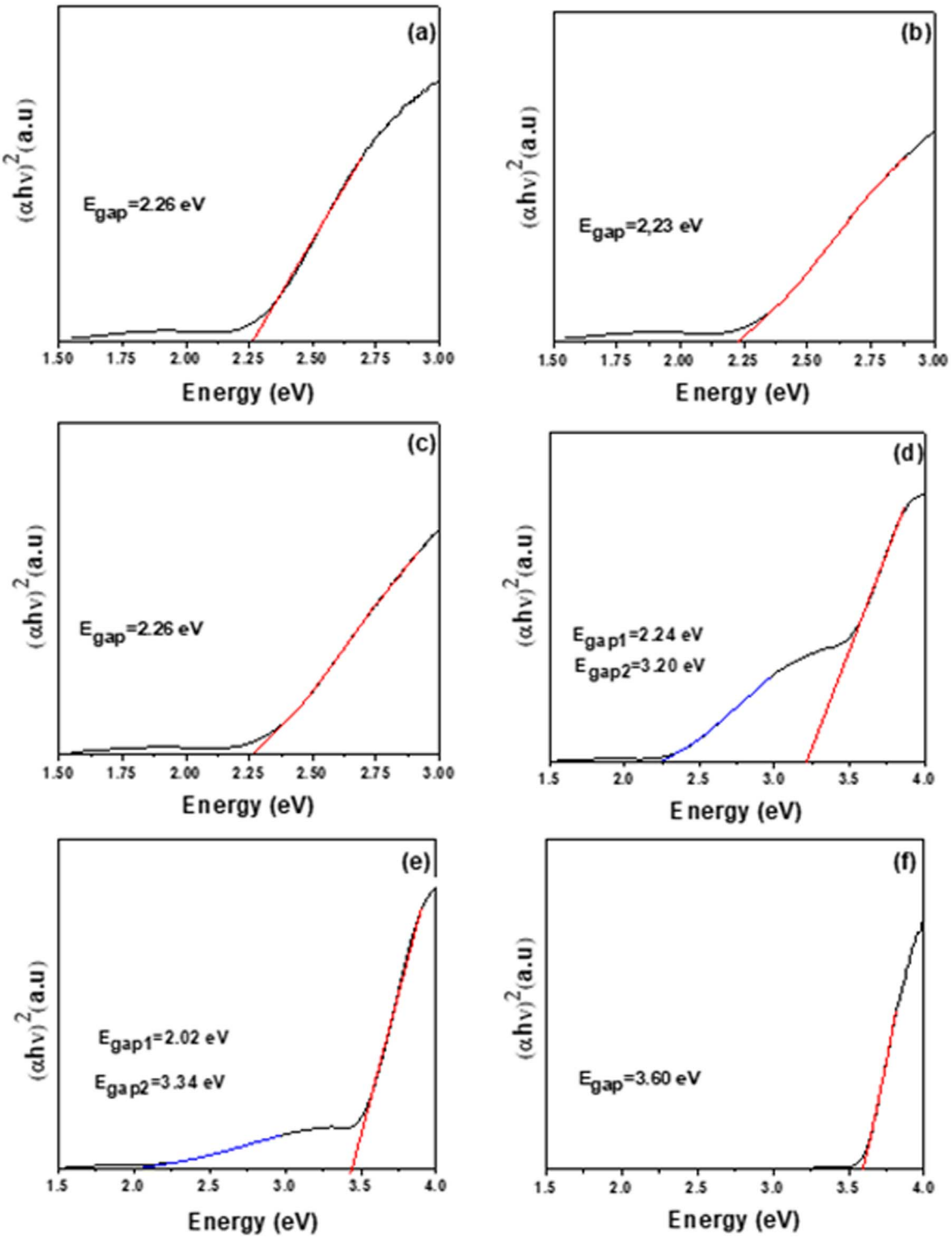

Fig. 4. UV–vis absorbance spectrum of ceramic powders based on $CaSr_xCu_{3-x}Ti_4O_{12}$, where (a) x = 0.00; (b) x = 0.15; (c) x = 0.30; (d) x = 1.50; (e) x = 2.70 e (f) x = 3.00.

emission of high energy in the blue region, caused by a stress generated in the c axis produced by the Sr^{2+}, whose ionic radius (1.26 Å) is larger when compared to the ionic radius of Cu^{2+} (0.73 Å) when the composition reaches x = 1.50 [48,49]. A phase transition from cubic to orthorhombic structure could be observed for the sample with x = 2.70 and is addressed to P8 Raman mode. The 13 vibrational Raman modes are evident for the sample with x = 3.00, indicating low symmetry at short-range. However, it is necessary to highlight that the mode located near 549 cm^{-1}, which is related to TO_4 phonon mode, usually found in the rhombohedral structure of SCTO (Fig. 3b), is evident for the samples with x = 2.70 and 3.00 [49]. The vibration Raman modes P12, P13 (740 cm^{-1} and 802 cm^{-1}) are associated to acoustic modes with high magnitude. All modes pointed out in this research were compared with the values related in the literature [48,50] (Table 2). The main differences observed could be caused by a structural disorder at short range in the structure, which is minimized when Cu^{2+} is substituted by Sr^{2+}.

3.4. Ultraviolet-Visible absorbance spectroscopy (UV–vis)

Fig. 4 shows the UV–vis spectra for the Sr^{2+} modified $CaSr_xCu_{3-x}Ti_4O_{12}$ ceramic powders. The optical band gap values obtained through the linear fitting of tails from the UV–vis spectra are shown. It is noted that samples with Sr^{2+} content of x = 0.00, 0.15 and 0.30 have an energy gap, around of 2.24 eV, due to the electronic transitions between the oxygen orbitals in the valence band (VB) and the copper orbitals in the conduction band (CB) corresponding to the CCTO phase [51]. On the other hand, for the samples with x = 1.50, 2.70 and 3.00, an energy gap at around 3.45 eV, can be attributed to the electronic transitions in the [TiO_6] clusters caused by charge transfer between the O-2p orbitals in the VB and Ti-3d orbitals in the CB [29].

Fig. 5 illustrates the dependence of band gap energy as a function of Sr^{2+} content. It can be noted that the band gap energy is quite similar for the samples with x = 0.00, 0.15 and 0.30 because the major phase present in such compositions is the CCTO phase, as previously discussed by Rietveld analysis. The same trend can be noted for the samples with x = 1.50, 2.70 and 3.00 of Sr^{2+} whereas the major phase is the SCTO. In this way, it can be concluded that the addition of Sr^{2+} in the CCTO generates a material with lower symmetry at short range as evidenced by Raman spectroscopy, and also with fewer defects producing an increase in the band gap energy. The samples with x = 1.50 and x = 2.70 had two band gaps, which are associated with the presence of different crystal structure as already reported in the literature [27]. Moreover, other authors have shown that small band gap values are characteristic

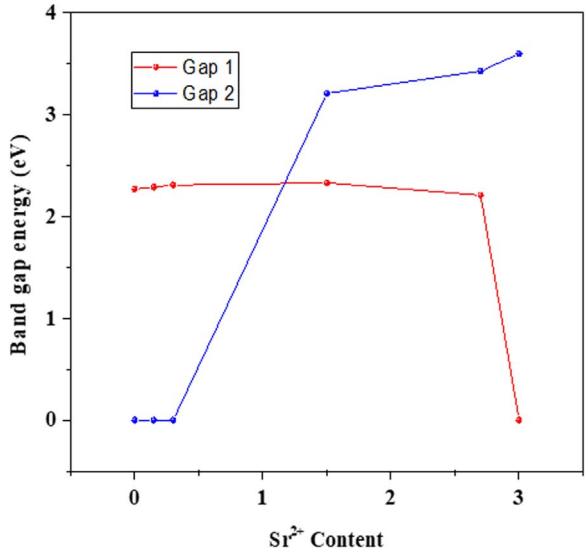

Fig. 5. Dependence of band gap energy as a function of Sr content based on $CaSr_xCu_{3-x}Ti_4O_{12}$ ($0.00 \leq x \leq 3.00$).

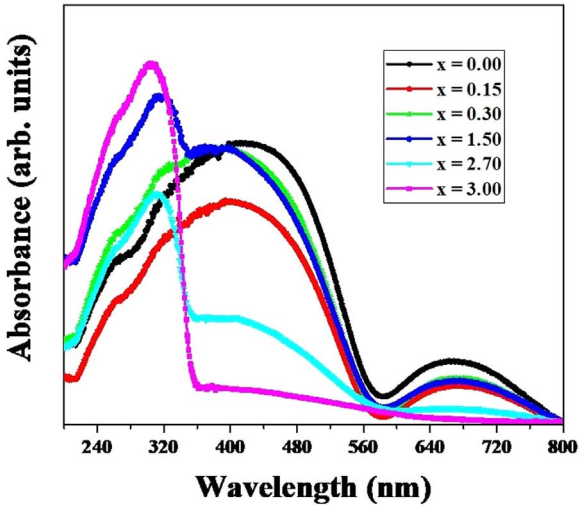

Fig. 6. Absorbance spectrum of ceramic powders based on $CaSr_xCu_{3-x}Ti_4O_{12}$ ($0.00 \leq x \leq 3.00$).

of structures with many defects, and the decrease of these defects produces an increase in the band gap [22,29,37].

The absorbance curves vs wavelength (nm) are presented in Fig. 6. It can be noted that the absorption process for the samples with x = 0.00, x = 0.15 and x = 0.30 began at 600 nm, which indicates that the energy gap is about 2.0 eV, as it was confirmed by UV–vis technique. This is typically associated with the CCTO cubic structure. On the other hand, the samples with x = 1.50 and x = 2.70 displayed a similar behavior, showing two absorption processes. The first one, near to 350 nm and the second, near to 600 nm, could be explained by two different crystal structures (cubic structure for CCTO), (and orthorhombic structure for CTO and SCTO phases), as previously discussed. An increase in the photon absorption was reached from a wavelength (350 nm), which corresponds to the energy of 3.0 eV, approximately. This value matches with the gap energy of the SCTO phase, present in the samples with higher Sr^{2+} contents. The samples with x = 2.70 showed a decrease in the photon absorption due to the decrease of CCTO phase. The sample with x = 3.00 showed a single SCTO photon absorption close to 350 nm, which indicates the presence of a single phase.

3.5. Photoluminescent spectroscopy

Fig. 7 shows the PL curves of the samples treated at 1050 °C and illustrates the effects of Sr^{2+} modified $CaSr_xCu_{3-x}Ti_4O_{12}$ ceramic powders. Samples with x = 0.00, x = 0.15 and x = 0.30 (Fig. 6a-c) has a broad emission near to the blue region (450 nm), which should be explained, according to T. Badapanda's and L. S. Cavalcante's works, by the presence of oxygen vacancies, produced in ternary oxides with changes in the temperature [51,52], On the other hand, the sample with x = 1.50 (Fig. 6d) shows no emission in the violet region being associated to deep defects in the band gap, whereas the samples with x = 2.70 and x = 3.00 (Fig. 6e-f) produce emissions in the violet and blue regions corresponding to shallow defects in the band gap [53]. Something that must be considered is that the decrease of the green emission with the increase in the amount of Sr^{2+} can be associated to the decrease of self-trapped charges, less interaction between electron and hole, and donor–acceptor recombination [54]. The orange-red emission was evidenced in all samples, beginning with an emission in the region near to the red region, and with the increase Sr^{2+} content this emission moves to the orange region, which is associated with shallow defects [52]. The results of this study reveal a positive influence of the Sr^{2+} ions on optical properties. Such doping leads to an increase in the band gaps which stimulates PL emission at different wavelengths

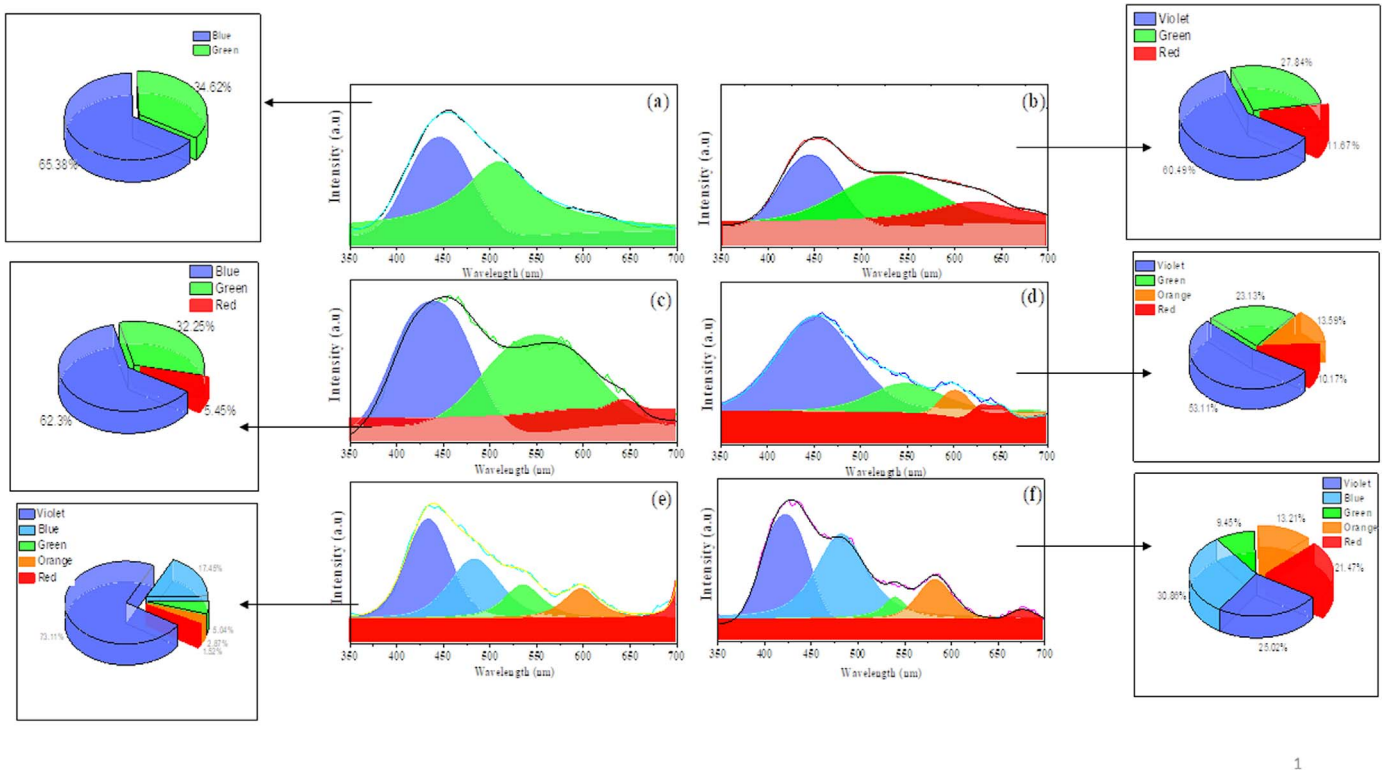

Fig. 7. Photoluminescent spectrum of ceramic powders based on $CaSr_xCu_{3-x}Ti_4O_{12}$ ($0.00 \leq x \leq 3.00$).

characterized by deep and shallow defects attributed to V_O and V_O vacancies. Thus, electronic transitions of low energies were higher in samples with Sr^{2+} addition. Typically, oxygen vacancies are the main responsible for the PL property representing the energetic levels in the band gap region causing charge transfer [29,34]. T. Sequinel et al. obtained CCTO thin films using a soft chemical solution and pressure method. The authors proposed that the pressure causes a decrease in the band gap and an increase in the photoluminescence (PL) emission suggesting that the pressure facilitates the displacement of Ti^{4+} in the titanate clusters, and the charge transference which could be attributed to the presence $[TiO_6]_o^x$ and $[TiO_5{\cdot}V_O^X]_d$ clusters (where o-order and d-disorder) in the structure [24,31]. It is known in the literature that the photoluminescence emission in the blue region is related to $[TiO_6]_o^x$ cluster with oxygen vacancies of the mono-ionized type [55], as can be seen with the Kröger-Vink notation through to the Eq. (2):

$$[TiO_6]^x + [TiO_5{\cdot}V_O^x] \rightarrow [TiO_6]' + [TiO_5{\cdot}V_O^{\bullet}], \quad (2)$$

while the emission in the lower energy region, green and red, is related to the charge transfer to clusters with doubly ionized vacancies (Eq. (3)):

$$[TiO_6]^x + [TiO_5{\cdot}V_O^{\bullet}] \rightarrow [TiO_6]' + [TiO_5{\cdot}V_O^{\bullet\bullet}]; \quad (3)$$

lower band gaps and intermediate energy levels produced PL emissions.

Our results pointed out that the samples with x = 0.15 to x = 1.5 possess a gradual increase of the emission in the blue region. Raman, XRD and UV–Vis spectroscopy data indicated that Sr2 + promotes an increased stress along the c axis of the crystal lattice with the coexistence of CCTO, SCTO and CTO phases, and photons absorption close to 2.25 eV. That indicates that the disorder state of the clusters in the structure tend to maintain the presence of shallow defects in the material, especially mono-ionized oxygen vacancies V_O. Higher Sr2 + content samples (x = 2.70–3.00) shows the absence of the CCTO phase with photons absorption of high energy in the range of 3.5 eV and a clear indication by Raman spectroscopy of less ordered symmetry. This reflects in the PL behavior, contributing to the emission in the blue, green and orange wavelengths. Therefore, the system with high Sr2 + content will be characterized by deep and shallow defects attributed to V_O and V_O vacancies [33,56–58].

4. Conclusions

Distinct PL responses were observed for Sr^{2+} modified $CaSr_xCu_{3-x}Ti_4O_{12}$ powders obtained through solid-state reaction. Sr^{2+} exerted a greater influence on optical characteristics which produced an increase in the band gap due to the rupture of the Ti–O bonds and the genesis of intermediary energy levels inside the band gap region (overlap between valence and conduction bands). A less ordered structure evidenced by high number of longitudinal and transversal modes were noted. High band gap energy values obtained by Sr^{2+} addition reveal a less ordered structure at short range with fewer defects than the CCTO system. Strontium doping leads to an increase in the band gaps which stimulates PL emission at different wavelengths characterized by deep and shallow defects attributed to V_O and V_O vacancies. This is caused by the absence of the CCTO phase with photons absorptions of high energy in the range of 3.5 eV and a clear indication of less ordered symmetry.

Acknowledgements

The authors would like to warmly express their gratitude and indebtedness to the São Paulo Research Foundation (FAPESP) (Grant CEPID/CDMF – FAPESP: 2013/07296-2) and the National Council for Scientific and Technological Development CAPES for the financial support granted during this research. The authors also thank Gabriel Cotrim Peinado for the contributions in this work.

References

[1] M.A. Subramanian, D. Li, N. Duan, B.A. Reisner, A.W. Sleight, High dielectric constant in ACu3Ti4O12 and $ACu_3Ti_3FeO_{12}$ phases, J. Solid State Chem. 151 (2000) 323–325, http://dx.doi.org/10.1006/jssc.2000.8703.
[2] S.-Y. Chung, I.-D. Kim, S.-J.L. Kang, Strong nonlinear current-voltage behaviour in perovskite-derivative calcium copper titanate, Nat. Mater. 3 (2004) 774–778, http://dx.doi.org/10.1038/nmat1238.

[3] H.-T. Jeng, G.Y. Guo, First-principles study of the structure and lattice dielectric response of $CaCu_3Ti_4O_{12}$, Phys. Rev. B 65 (2002) 94429, http://dx.doi.org/10.1103/PhysRevB.65.094429.

[4] J. Zhao, J. Liu, G. Ma, Preparation, characterization and dielectric properties of $CaCu_3Ti_4O_{12}$ ceramics, Ceram. Int. 38 (2012) 1221–1225, http://dx.doi.org/10.1016/j.ceramint.2011.08.052.

[5] J. Li, T. Xu, S. Li, H. Jin, W. Li, Structure and electrical response of $CaCu_3Ti_4O_{12}$ ceramics: effect of heat treatments at the high vacuum, J. Alloy. Compd. 506 (2010) L1–L4, http://dx.doi.org/10.1016/j.jallcom.2010.06.155.

[6] M.A. Subramanian, A.W. Sleight, $ACu_3Ti_4O_{12}$ and $ACu_3Ru_4O_{12}$ perovskites: high dielectric constants and valence degeneracy, Solid State Sci. (2002), http://dx.doi.org/10.1016/S1293-2558(01)01262-6.

[7] T. Li, R. Xue, J. Hao, Y. Xue, Z. Chen, The effect of calcining temperatures on the phase purity and electric properties of $CaCu_3Ti_4O_{12}$ ceramics, J. Alloy. Compd. (2011), http://dx.doi.org/10.1016/j.jallcom.2010.09.163.

[8] Y. Huang, L. Liu, D. Shi, S. Wu, S. Zheng, L. Fang, C. Hu, B. Elouadi, Giant dielectric permittivity and non-linear electrical behavior in $CaCu_3Ti_4O_{12}$ varistors from the molten-salt synthesized powder, Ceram. Int. (2013), http://dx.doi.org/10.1016/j.ceramint.2013.01.023.

[9] M.A. Ramírez, P.R. Bueno, J.A. Varela, E. Longo, Non-Ohmic and dielectric properties of a $Ca_2Cu_2Ti_4O_{12}$ polycrystalline system, Appl. Phys. Lett. 89 (2006) 10–13, http://dx.doi.org/10.1063/1.2393122.

[10] D.C. Sinclair, T.B. Adams, F.D. Morrison, A.R. West, $CaCu_3Ti_4O_{12}$: one-step internal barrier layer capacitor, Appl. Phys. Lett. 80 (2002) 2153–2155, http://dx.doi.org/10.1063/1.1463211.

[11] R.B. Paulo, T. Ronald, P. Rodrigo, J. Ednan, A.R. Miguel, C.R. Willian, L. Elson, A.V. José, A polaronic stacking fault defect model for $CaCu_3Ti_4O_{12}$ material: an approach for the origin of the huge dielectric constant and semiconducting coexistent features, J. Phys. D: Appl. Phys. 42 (2009) 55404, http://dx.doi.org/10.1088/0022-3727/42/5/055404.

[12] W.C. Ribeiro, E. Joanni, R. Savu, P.R. Bueno, Nanoscale effects and polaronic relaxation in $CaCu_3Ti_4O_{12}$ compounds, Solid State Commun. 151 (2011) 173–176, http://dx.doi.org/10.1016/j.ssc.2010.10.034.

[13] X.H. Zheng, C. Zhang, B.L. Liang, D.P. Tang, X. Huang, X.L. Liu, An effective way to tune the microstructure and dielectric properties of $CaCu_3Ti_4O_{12}$ ceramics, J. Alloy. Compd. 505 (2010) 10–14, http://dx.doi.org/10.1016/j.jallcom.2010.06.060.

[14] M.A. Subramanian, A.W. Sleight, $ACu_3Ti_4O_{12}$ and $ACu_3Ru_4O_{12}$ perovskites: high dielectric constants and valence degeneracy, Solid State Sci. 4 (2002) 347–351, http://dx.doi.org/10.1016/S1293-2558(01)01262-6.

[15] L. He, J.B. Neaton, M.H. Cohen, D. Vanderbilt, C.C. Homes, First-principles study of the structure and lattice dielectric response of $CaCu_3Ti_4O_{12}$, 22 (n.d.). doi:10.1103/PhysRevB.65.214112.

[16] D.C. Sinclair, T.B. Adams, F.D. Morrison, A.R. West, $CaCu_3Ti_4O_{12}$: One-step internal barrier layer capacitor, Appl. Phys. Lett. 80 (2002) 2153–2155, http://dx.doi.org/10.1063/1.1463211.

[17] P.R. Bueno, R. Tararan, R. Parra, E. Joanni, M.A. Ramirez, W.C. Ribeiro, E. Longo, A polaronic stacking fault defect model for $CaCu_3Ti_4O_{12}$ material: an approach for the origin of the huge dielectric constant and semiconducting coexistent features e A Varela, 55404 (n.d.). doi:<http://dx.doi.org/10.1088/0022-3727/42/5/055404>.

[18] D. Xu, L. Shi, Z. Wu, Q. Zhong, X. Wu, Microstructure and electrical properties of ZnO-Bi_2O_3-based varistor ceramics by different sintering processes, J. Eur. Ceram. Soc. (2009), http://dx.doi.org/10.1016/j.jeurceramsoc.2008.10.020.

[19] C.B. Samantaray, M.L. Nanda Goswami, D. Bhattacharya, S.K. Ray, H.N. Acharya, Photoluminescence properties of Eu^{3+}-doped barium strontium titanate (Ba, Sr)TiO_3 ceramics, Mater. Lett. 58 (2004) 2299–2301, http://dx.doi.org/10.1016/j.matlet.2004.03.001.

[20] J. Zhao, J. Liu, G. Ma, Preparation, characterization and dielectric properties of $CaCu_3Ti_4O_{12}$ ceramics, Ceram. Int. 38 (2011) 1221–1225, http://dx.doi.org/10.1016/j.ceramint.2011.08.052.

[21] A.T. De Figueiredo, V.M. Longo, R.O. Da Silva, V.R. Mastelaro, A. Mesquita, R.W.A. Franco, J.A. Varela, E. Longo, Structural XANES characterization of $Ca_{0.99}Sm_{0.01}TiO_3$ perovskite and correlation with photoluminescence emission, Chem. Phys. Lett. 544 (2012) 43–48, http://dx.doi.org/10.1016/j.cplett.2012.06.027.

[22] L.H. Oliveira, A.P. De Moura, T.M. Mazzo, M.A. Ramírez, L.S. Cavalcante, S.G. Antonio, W. Avansi, V.R. Mastelaro, E. Longo, J.A. Varela, Structural refinement and photoluminescence properties of irregular cube-like $(Ca_{1-x}Cu_x)TiO_3$ microcrystals synthesized by the microwave-hydrothermal method, Mater. Chem. Phys. 136 (2012) 130–139, http://dx.doi.org/10.1016/j.matchemphys.2012.06.042.

[23] A.E. Souza, R.A. Silva, G.T.A. Santos, S.R. Teixeira, S.G. Antonio, M.L. Moreira, D.P. Volanti, E. Longo, Order-disorder degree of self-assembled clusters: influence on photoluminescence emission and morphology of $Ba_xSr_{1-x}TiO_3$ nanocrystals, Chem. Phys. Lett. 514 (2011) 301–306, http://dx.doi.org/10.1016/j.cplett.2011.08.045.

[24] G.K. Ribeiro, F.S. Vicente, M.I.B. Bernardi, A. Mesquita, Short-range structure and photoluminescent properties of the $CaTiO_3$:Pr, La phosphor, J. Alloy. Compd. 688 (2016) 497–503, http://dx.doi.org/10.1016/j.jallcom.2016.07.090.

[25] H. Zheng, G.D.C. Csete de Györgyfalva, R. Quimby, H. Bagshaw, R. Ubic, I.M. Reaney, J. Yarwood, Raman spectroscopy of B-site order-disorder in $CaTiO_3$-based microwave ceramics, J. Eur. Ceram. Soc. 23 (2003) 2653–2659, http://dx.doi.org/10.1016/S0955-2219(03)00149-3.

[26] L.S. Cavalcante, N.C. Batista, T. Badapanda, M.G.S. Costa, M.S. Li, W. Avansi, V.R. Mastelaro, E. Longo, J.W.M. Espinosa, M.F.C. Gurgel, Local electronic structure, optical bandgap and photoluminescence (PL) properties of $Ba(Zr_{0.75}Ti_{0.25})O_3$ powders, Mater. Sci. Semicond. Process. 16 (2013) 1035–1045, http://dx.doi.org/10.1016/j.mssp.2012.12.010.

[27] L.H. Oliveira, A.P. De Moura, F.A. La Porta, I.C. Nogueira, E.C. Aguiar, T. Sequinel, I.L.V. Rosa, E. Longo, J.A. Varela, Influence of Cu-doping on the structural and optical properties of $CaTiO_3$ powders, Mater. Res. Bull. 81 (2016) 1–9, http://dx.doi.org/10.1016/j.materresbull.2016.04.024.

[28] G. Li, Z. Yin, M. Zhang, Study on optical and dielectric properties of $CaCu_3Ti_4O_{12}$ by first-principles calculation, Mater. Sci. Eng.: B. 150 (2008) 163–167, http://dx.doi.org/10.1016/j.mseb.2008.04.006.

[29] L.H. Oliveira, E.C. Paris, W. Avansi, M.A. Ramirez, V.R. Mastelaro, E. Longo, J.A. Varela, Correlation between photoluminescence and structural defects in $Ca_{1+x}Cu_{3-x}Ti_4O_{12}$ systems, J. Am. Ceram. Soc. 96 (2013) 209–217, http://dx.doi.org/10.1111/jace.12020.

[30] F. Moura, A.Z. Simões, R.C. Deus, M.R. Silva, J.A. Varela, E. Longo, Intense photoluminescence emission at room temperature in calcium copper titanate powders, Ceram. Int. 39 (2013) 3499–3506, http://dx.doi.org/10.1016/j.ceramint.2012.11.034.

[31] T. Sequinel, I.G. Garcia, S.M. Tebcherani, E.T. Kubaski, L.H. Oliveira, M. Siu Li, E. Longo, J.A. Varela, Red shift and higher photoluminescence emission of CCTO thin films undergoing pressure treatment, J. Alloy. Compd. 583 (2014) 488–491, http://dx.doi.org/10.1016/j.jallcom.2013.08.210.

[32] L.H. Oliveira, M.A. Ramirez, M.A. Ponce, L.A. Ramajo, A.R. Albuquerque, J.R. Sambrano, E. Longo, M.S. Castro, F.A. La Porta, Optical and gas-sensing properties, and electronic structure of the mixed-phase $CaCu_3Ti_4O_{12}/CaTiO_3$ composites, Mater. Res. Bull. 93 (2017) 47–55, http://dx.doi.org/10.7498/aps.62.087701.

[33] V.M. Longo, A.T. De Figueiredo, S. De Lázaro, M.F. Gurgel, M.G.S. Costa, C.O. Paiva-Santos, J.A. Varela, E. Longo, V.R. Mastelaro, F.S. De Vicente, A.C. Hernandes, R.W.A. Franco, Structural conditions that leads to photoluminescence emission in $SrTiO_3$: an experimental and theoretical approach, J. Appl. Phys. 104 (2008), http://dx.doi.org/10.1063/1.2956741.

[34] R. Parra, E. Joanni, J.W.M. Espinosa, R. Tararam, M. Cilense, P.R. Bueno, J.A. Varela, E. Longo, Photoluminescent $CaCu_3Ti_4O_{12}$-based thin films synthesized by a sol-gel method, J. Am. Ceram. Soc. 91 (2008) 4162–4164, http://dx.doi.org/10.1111/j.1551-2916.2008.02817.x.

[35] A.F.L. Almeida, P.B.A. Fechine, J.C. Góes, M.A. Valente, M.A.R. Miranda, A.S.B. Sombra, Dielectric properties of $BaTiO_3$ (BTO)-$CaCu_3Ti_4O_{12}$ (CCTO) composite screen-printed thick films for high dielectric constant devices in the medium frequency (MF) range, Mater. Sci. Eng. B: Solid-State Mater. Adv. Technol. 111 (2004) 113–123, http://dx.doi.org/10.1016/j.mseb.2004.03.027.

[36] J.H. Clark, M.S. Dyer, R.G. Palgrave, C.P. Ireland, J.R. Darwent, J.B. Claridge, M.J. Rosseinsky, Visible light photo-oxidation of model pollutants using $CaCu_3Ti_4O_{12}$: an experimental and theoretical study of optical properties, Electron. Struct., Sel., J. Am. Chem. Soc. 133 (2011) 1016–1032, http://dx.doi.org/10.1021/ja1090832.

[37] F. Moura, A.C. Cabral, L.S.R. Rocha, E.C. Aguiar, A.Z. Simões, E. Longo, Photoluminescence emission in zirconium-doped calcium copper titanate powders, Ceram. Int. 42 (2016) 4837–4844, http://dx.doi.org/10.1016/j.ceramint.2015.11.169.

[38] T. Li, D. Liu, H. Dai, H. Xiang, Z. Chen, H. He, Z. Chen, Effect of defect on the nonlinear and dielectric property of $Ca_{(1-x)}Sr_xCu_3Ti_4O_{12}$ ceramics synthesized by sol–gel process, J. Alloy. Compd. 599 (2014) 145–149, http://dx.doi.org/10.1016/j.jallcom.2014.02.076.

[39] V. Vidyadharan, E. Sreeja, S.K. Jose, C. Joseph, N.V. Unnikrishnan, P.R. Biju, Spectroscopic and photoluminescence characterization of Dy^{3+} in $Sr_{0.5}Ca_{0.5}TiO_3$ phosphor, Luminescence 31 (2016) 202–209, http://dx.doi.org/10.1002/bio.2946.

[40] V. Vidyadharan, K.P. Mani, M.S. Sajna, C. Joseph, N.V. Unnikrishnan, P.R. Biju, Synthesis and luminescence characterization of Pr^{3+} doped $Sr_{1.5}Ca_{0.5}SiO_4$ phosphor, Spectrochim. Acta - Part A: Mol. Biomol. Spectrosc. 133 (2014) 767–772, http://dx.doi.org/10.1016/j.saa.2014.06.016.

[41] V. Vidyadharan, R. Mohan, C. Joseph, N.V. Unnikrishnan, P.R. Biju, Luminescent characteristics of UV excited $Sr_{0.5}Ca_{0.5}TiO_3$: Pr^{3+} reddish-orange phosphor, Mater. Chem. Phys. 170 (2016) 38–43, http://dx.doi.org/10.1016/j.matchemphys.2015.12.016.

[42] X. Huang, H. Zhang, M. Wei, Y. Lai, J. Li, Effect of semiconductive grain and microstructure on the dielectric properties of $CaCu_3Ti_4O_{12}$ ceramics with Sr^{2+} doping, J. Alloy. Compd. (2017), http://dx.doi.org/10.1016/j.jallcom.2017.03.096.

[43] P. Ptáček, E. Bartoníčková, J. Švec, T. Opravil, F. Šoukal, F. Frajkorová, The kinetics and mechanism of thermal decomposition of $SrCO_3$ polymorphs, Ceram. Int. 41 (2014) 115–126, http://dx.doi.org/10.1016/j.ceramint.2014.08.043.

[44] X.G. Li, Y. Lv, B.G. Ma, W.Q. Wang, S.W. Jian, Decomposition kinetic characteristics of calcium carbonate containing organic acids by TGA, Arab. J. Chem. 3 (2013), http://dx.doi.org/10.1016/j.arabjc.2013.09.026.

[45] F. Cerdeira, C.J. Buchenauer, F.H. Pollak, M. Cardona, Stress-induced shifts of first-order Raman frequencies of diamond- and zinc-blende-type semiconductors, Phys. Rev. B 5 (1972) 580–593, http://dx.doi.org/10.1103/PhysRevB.5.580.

[46] C.J. Howard, R.L. Withers, B.J. Kennedy, Space group and structure for the perovskite $Ca_{0.5}Sr_{0.5}TiO_3$, J. Solid State Chem. 160 (2001) 8–12, http://dx.doi.org/10.1006/jssc.2001.9229.

[47] A.K. Rai, K.D. Mandal, D. Kumar, O. Parkash, Characterization of nickel doped CCTO: $CaCu_{2.9}Ni_{0.1}Ti_4O_{12}$ and $CaCu_3Ti_{3.9}Ni_{0.1}O_{12}$ synthesized by semi-wet route, J. Alloy. Compd. (2010), http://dx.doi.org/10.1016/j.jallcom.2009.10.247.

[48] A.F.L. Almeida, P.B.A. Fechine, M.P.F. Graça, M.A. Valente, A.S.B. Sombra, Structural and electrical study of $CaCu_3Ti_4O_{12}$ (CCTO) obtained in a new ceramic procedure, J. Mater. Sci.: Mater. Electron. (2009), http://dx.doi.org/10.1007/s10854-008-9675-4.

[49] D.A. Tenne, A.M. Clark, A.R. James, K. Chen, X.X. Xi, Soft phonon modes in

$Ba_{0.5}Sr_{0.5}TiO_3$ thin films studied by Raman spectroscopy, Appl. Phys. Lett. 79 (2001) 3836–3838, http://dx.doi.org/10.1063/1.1424463.

[50] A. Koitzsch, G. Blumberg, A. Gozar, B. Dennis, A.P. Ramirez, S. Trebst, S. Wakimoto, Antiferromagnetism in $CaCu_3Ti_4O_{12}$ studied by magnetic Raman spectroscopy, Phys. Rev. B (2002) 52406, http://dx.doi.org/10.1103/PhysRevB.65.052406.

[51] S.B. Fagan, A.G.S. Filho, A.P. Ayala, J.M. Filho, Ab initio calculations of $CaCu_3Ti_4O_{12}$ under high pressure: structural and electronic properties, Phys. Rev. B 72 (2005) 14106, http://dx.doi.org/10.1103/PhysRevB.72.014106.

[52] T. Badapanda, S.K. Rout, L.S. Cavalcante, J.C. Sczancoski, S. Panigrahi, E. Longo, M.S. Li, Optical and dielectric relaxor behaviour of $Ba(Zr_{0.25}Ti_{0.75})O_3$ ceramic explained by means of distorted clusters, J. Phys. D: Appl. Phys. 42 (2009), http://dx.doi.org/10.1088/0022-3727/42/17/175414.

[53] L.S. Cavalcante, J.C. Sczancoski, J.W.M. Espinosa, V.R. Mastelaro, A. Michalowicz, P.S. Pizani, F.S. De Vicente, M.S. Li, J.A. Varela, E. Longo, Intense blue and green photoluminescence emissions at room temperature in barium zirconate powders, J. Alloy. Compd. 471 (2009) 253–258, http://dx.doi.org/10.1016/j.jallcom.2008.03.080.

[54] L. Zhang, J. Wang, D. Peng, F. Long, S. Mo, Y. Wu, Z. Zou, Photoluminescence and dielectric properties of pure/Yb-doped $SrZrO_3$ crystals, J. Phys. Chem. Solids 104 (2017) 1–7, http://dx.doi.org/10.1016/j.jpcs.2017.01.002.

[55] R.A.C. Amoresi, V. Teodoro, G.F. Teixeira, M.S. Li, A.Z. Simões, L.A. Perazolli, E. Longo, M.A. Zaghete, Electrosteric colloidal stabilization for obtaining $SrTiO_3$/TiO_2 heterojunction: microstructural evolution in the interface and photonics properties, J. Eur. Ceram. Soc. (2017), http://dx.doi.org/10.1016/j.jeurceramsoc.2017.10.056.

[56] M. Mondego, R.C. de Oliveira, M. Penha, M.S. Li, E. Longo, Blue and red light photoluminescence emission at room temperature from $CaTiO_3$ decorated with α-Ag_2WO_4, Ceram. Int. 43 (2017) 5759–5766, http://dx.doi.org/10.1016/j.ceramint.2017.01.121.

[57] A.E. Souza, G.T.A. Santos, B.C. Barra, W.D. Macedo, S.R. Teixeira, C.M. Santos, a.M.O.R. Senos, L. Amaral, E. Longo, Photoluminescence of $SrTiO_3$: influence of Particle size and morphology, Cryst. Growth Des. 12 (2012) 5671–5679, http://dx.doi.org/10.1021/cg301168k.

[58] A.F.L. Almeida, P.B.A. Fechine, J.C. Góes, M.A. Valente, M.A.R. Miranda, A.S.B. Sombra, Dielectric properties of $BaTiO_3$ (BTO)-$CaCu_3Ti_4O_{12}$ (CCTO) composite screen-printed thick films for high dielectric constant devices in the medium frequency (MF) range, Mater. Sci. Eng. B: Solid-State Mater. Adv. Technol. (2004), http://dx.doi.org/10.1016/j.mseb.2004.03.027.